International Journal of Thermal Sciences 77 (2014) 1–10

Contents lists available at ScienceDirect

International Journal of Thermal Sciences

journal homepage: www.elsevier.com/locate/ijts

Numerical study on thermal stresses of a planar solid oxide fuel cell

Pengfei Fan, Guojun Li, Yikai Zeng, Xiongwen Zhang*

Key Laboratory of Thermo-Fluid Science and Engineering of MOE, School of Energy and Power Engineering, Xi'an Jiaotong University, Xi'an, Shaanxi 710049, China

ARTICLE INFO

Article history:
Received 3 February 2013
Received in revised form
10 October 2013
Accepted 15 October 2013
Available online

Keywords:
Solid oxide fuel cell
Numerical simulation
Thermal stress

ABSTRACT

A three-dimensional (3D) finite element model consists of positive electrode–electrolyte–negative electrode (PEN) and metallic interconnect (MIC) assembly is constructed by using commercial finite element software Abaqus. With the simulated temperature profile in the planar solid oxide fuel cell (SOFC), the finite element method is employed to calculate the thermal stress distribution in a planar SOFC. The effects of temperature profile, electrodes and electrolyte thickness, and coefficients of thermal expansion (CTEs) mismatch between components are characterized. The value and distribution of thermal stress are the functions of the applied materials CTEs, applied temperature profiles and thickness of anode and electrolyte. The calculated results can be applied as the guide for SOFC materials selection and SOFC structure design. The anode is subjected to large tensile stresses and the electrolyte is subjected to large compressive stresses during the first cooling from the sintering temperature. The chemical reduction of NiO to Ni in the porous anode lowers the absolute stress level in the PEN structure by 20%. The large tensile stresses in the anode and the large compressive stresses in the electrolyte relax partly when the SOFC operates at high temperature. Cracks could probably appear in the anode structure when the PEN structure is cooling to room temperature after the sintering.

1. Introduction

Fuel cells are the most efficient devices for the electrochemical conversion of chemical energy of hydrogen into electricity, and have been gaining increasing attention in recent years for environmentally friendly with little or no toxic emission and efficient distributed power generation. In the existing fuel cells, the solid oxide fuel cell (SOFC) with monolithic, planar and tubular geometries, as a high temperature fuel cell, makes a good performance in power generation and continues to show great promise as a future power source. In SOFC stack designs, the planar type design has received much attention recently, because it is simpler to fabricate and easier to be made into various shapes than the other type designs. Besides, the planar type SOFC offers higher power density relative to the tubular type SOFC due to the low electrical resistance as a result of the shorter current paths. A typical operating temperature of a solid oxide fuel cell is 600 °C–1000 °C, which leads to severe thermal stresses and warpage on the positive electrode–electrolyte–negative electrode (PEN) structures of SOFCs caused by the mismatch of the coefficients of thermal expansion (CTEs) of various layers in the PEN structures of SOFCs due to the temperature changes during the PEN manufacturing process and thermal cycling. And these may lead to cracks and destroy the SOFC structure.

Numerical studies were conducted by many investigators on electric performance of SOFC using simplified electrochemical models [1–3], e.g. the Tafel equation, which is linear of Butler-Volmer equation, is widely used for activation polarization calculation. For the model of concentration polarization, the Knudsen diffusion was neglected for gas diffusion through the porous electrodes [2,3]. Ferguson et al. [4] presented a numerical model with solving both flow equations and potential equation for various geometries of SOFCs. The thermo-fluid analysis of a planar SOFC was performed using the computational fluid dynamics tool `STAR-CD' by Yakabe et al. [5]. Since SOFCs operate at high temperature and the cell scale is tiny, experimental studies on the thermal stresses is difficult. The X-ray computer tomography was used to permit an assessment of the maximum defect size by Malzbender et al. [6]. The residual stress in the electrodes was estimated by curvature measurement by Selcuk et al. [7]. The X-ray diffraction method was used to measure the residual stresses in the electrolyte of the anode-supported cell by Yakabe et al. [8] and Fischer et al. [9]. Most advanced researches of thermal stresses of SOFC were made

* Corresponding author. Tel.: +86 29 82665447; fax: +86 29 82665062.
E-mail addresses: Pengfei.v@Gmail.com (P. Fan), liguojun@mail.xjtu.edu.cn (G. Li), xwenz@mail.xjtu.edu.cn, xiongwenz@gmail.com (X. Zhang).

1290-0729/$ – see front matter © 2013 Elsevier Masson SAS. All rights reserved.
http://dx.doi.org/10.1016/j.ijthermalsci.2013.10.008

by establishing computer models and numerical simulations. Numerical studies for SOFC thermal stresses were conducted by different investigators. A two-dimensional model, based on the finite volume method, was developed in FORTRAN for simulation of a planar electrolyte supported SOFC by Selimovic et al. [10]. A 2-D mathematical model was developed to estimate the thermal stresses and to predict the lifetime of the cell [11] and the Weibull theory was used to predict the risk of cell degradation based on the 2-D calculation of stress field [12]. A stack modeling framework that combines thermo-electrochemical models, including degradation and a contact finite-element thermo-mechanical model based on an anode-supported SOFC was used to study the mechanical reliability and durability of SOFC stacks by Nakajo et al. [13,14]. The ANSYS software was used to carry out three-dimensional (3D) finite element analyses of SOFC bonded compliant seal designs by Weil et al. [15] and Jiang et al. [16].

The purpose of the present work is to study the thermal stresses in the SOFC components using a three-dimensional (3D) model simulation. In order to derive the stresses, a 3D numerical model of SOFCs for various geometries with complete polarization is employed in this study including methane reforming and the water-gas shift. This model is coupled with the governing equations through the user defined function (UDF) interface provided by the commercial computational fluid dynamics (CFD) software, Fluent. Transport equations for mass, momentum, species, energy and electrical potential are solved using the software, Fluent. The electric characteristics of the conductive components and the profile characteristics of the temperature for the planar configured SOFC are studied. A 3D finite element thermal stresses model consists of PEN and interconnects assembly is constructed by using the commercial finite element analysis (FEA) software Abaqus based on the temperature profile in the planar SOFC calculated by the electrochemical model. The effects of temperature profile, electrodes and electrolyte thicknesses and CTE mismatches between components are characterized. The calculated results can be applied as the guide for the SOFC materials selection and the SOFC structure design to improve the SOFC structural performance and its reliability.

2. Mathematical model

2.1. Model geometry

A fuel cell stack modeling exercise was conducted by International Energy Agency (IEA) involving seven European countries and Japan in 1995. Two cases of SOFC stack operation were simulated: (1) one cell stack operating with humidified hydrogen fuel and air feed and (2) one cell stack operating with direct internal steam reforming of methane and air. These two cases were called “Benchmark Test 1” and “Benchmark Test 2” in the IEA database. In this work, a simplified single unit cell model with bipolar channels is studied. Furthermore, since the geometry of the single unit is symmetric, only half of the one repeating unit is simulated. The configuration of a half unit cell is illustrated in Fig. 1. Both co-flow and counter-flow planar SOFC are modeled in this work. The geometrical parameters of a single cell for the calculation are given as follows: channel reaction area 3 mm × 100 mm, channel height 1 mm, underneath MIC reaction area 2.42 mm × 100 mm, MIC rib width 2.42 mm, electrolyte thickness 150 μm, anode thickness 50 μm, cathode thickness 50 μm, and bipolar plate thickness 2.5 mm. As shown the half unit cell in Fig. 1, the active area in the numerical computation contains a half channel reaction area and a half underneath MIC reaction area, which equals to2.71 mm × 100 mm. The permeability of the porous electrode is 1×10^{-8}/m and the porosity is 0.2.

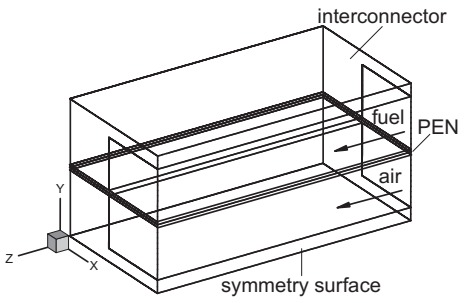

Fig. 1. The model geometry of the half single unit cell for the planar SOFC.

2.2. Electrochemical model

The electrochemical reactions taken into account in the SOFC are as follows:

$$\text{Anode side}: H_2 + O^{2-} \rightarrow H_2O + 2e^-$$

$$\text{Cathode side}: 1/2O^2 + 2e^- \rightarrow O^{2-}$$

$$\text{Overall reaction}: H_2 + O^{2-} \rightarrow H_2O + 2e^-$$

For the internal steam reforming of the SOFC, the reforming reaction and water-gas shift reaction are added within the anode:

$$\text{Methane steam reforming}: CH_4 + H_2O \rightarrow CO + 3H_2$$

$$\text{Water} - \text{gas shift}: H_2O + CO \rightarrow CO_2 + H_2$$

Electrochemical reactions were assumed to occur at the interfaces between electrodes and electrolyte. The shift reaction is fast enough and in this model we assume that the shift reaction is in chemical equilibrium in the anode.

As an energy conservation system, the voltage generated by the SOFC can be calculated by combining the energy conservation and entropy balance of the electrochemical reaction for the SOFC [17]. A complete polarization model is employed in this paper [18]. The voltage generated by SOFC is modeled as

$$E_v = -\frac{1}{z_e F}\left[\sum_i (\lambda_i g_i)_p - \sum_i (\lambda_i g_i)_r\right] - (\eta_{act} + \eta_{conc} + \eta_{ohm}) \tag{1}$$

where

$$g_i(T, p_i) = h_i(T) - Ts_i(T, p_i) = \int_{T_0}^{T} c_{pi}(T)\mathrm{d}T - T\int_{T_0}^{T} \frac{c_{pi}(T)}{T}\mathrm{d}T - RT\ln\frac{P_0}{p_i} \tag{2}$$

In the SOFC, the voltage losses include the activation polarization η_{act}, concentration polarization η_{conc} and ohmic polarization η_{ohm}.The activation polarization is the energy barrier existing between the electronic and the ionic conductors in the electrochemical reaction. The activation polarization occurs at both electrodes in all ranges of current density. It is calculated by the Butler–Volmer equation [26]. The transfer coefficient β is assumed to 0.5 in this work, the activation polarization can be calculated by

$$\eta_{act} = \frac{2RT}{n_e F}\sin h^{-1}\left(\frac{i}{2i_0}\right) \quad (3)$$

where the exchange current density i_0 depends on the partial pressure of reaction gas compositions and temperature. The Eqs. (4) and (5) are applied in the model according to Ref. [19].

At the anode side,

$$i_{0,a} = \gamma_a\left(\frac{p_{H_2}}{p_{ref}}\right)\left(\frac{p_{H_2O}}{p_{ref}}\right)\exp\left(-\frac{E_a}{RT}\right) \quad (4)$$

At the cathode side,

$$i_{0,c} = \gamma_c\left(\frac{p_{O_2}}{p_{ref}}\right)^{0.25}\exp\left(-\frac{E_c}{RT}\right) \quad (5)$$

The electrochemical reactions occur at the electrolyte–electrode interface. The reaction gas partial pressures change as the species diffuse through the porous material from gas channels to the reaction sites. The diffusion processes are described by both ordinary diffusion and Knudsen diffusion. The voltage loss due to the species diffusion resistance is called the concentration polarization, which occurs at both electrodes modeled as follows [18]:

$$\eta_{conc,a} = -\frac{RT}{2F}\left[\ln\left(\frac{p_{H_2}}{p^e_{H_2}}\right) - \ln\left(\frac{p_{H_2O}}{p^e_{H_2O}}\right)\right]$$
$$\eta_{conc,c} = -\frac{RT}{4F}\ln\left(\frac{p_{O_2}}{p^e_{O_2}}\right) \quad (6)$$

Ohmic losses, which arise from the resistance to electric charge conduction through cell components, depend linearly on current. The conductivity of the electric components is a function of temperature and can be calculated by the following equation:

$$\sigma = \frac{A_0}{T}\exp\left(-\frac{E_0}{kT}\right) \quad (7)$$

Therefore, the ohmic losses are written as:

$$\eta_{ohm} = \left|\vec{i}\cdot\vec{n}\right|r = \left|\vec{i}\cdot\vec{n}\right|l_{el}/\sigma \quad (8)$$

Due to the high operating temperature of SOFC, methane and water vapor in the fuel gas are adsorbed into anode and combine to produce hydrogen. The reaction rate for methane reforming used in the present model is shown in the following equation [3,20].

$$\dot{r}_R = k_0 p_{CH_4} f_e \exp\left(\frac{-\Delta E}{RT}\right) \quad (9)$$

where the equilibrium factor f_e is approximated as 1. The equilibrium constant for shift reaction is expressed as

$$K_{shift} = \exp\left(\frac{-\Delta G_{wgs}}{RT}\right) \quad (10)$$

where the change of Gibbs free energy (ΔG_{wgs}) is calculated by Eq. (2).

2.3. Thermo-fluid model

The thermo-fluids analysis is performed using the CFD software, Fluent. Thermodynamic equations for the electrochemical reactions and equations governing the conservation of mass, momentum, and energy are constructed and solved by the UDF. The standard $k-\varepsilon$ model and SIMPLEC algorithm are used.

The steady fluid flow governing equations can be written as follows:

$$\mathrm{div}\left(\rho\vec{V}\phi\right) = \mathrm{div}\left(\Gamma_\phi \mathrm{grad}\phi\right) + S_\phi \quad (11)$$

where Γ is the diffusion coefficient and S_φ is the source term for the generic variable φ. They are given in Ref. [21] for all conservation equations except the species transport equation and the electric potential equation. For the continuity equation, $\varphi = 1$. For the other conservation equations, φ equals Y_i the mass fraction of each species for the transport equations, V_j the velocity for each direction for the momentum equations, T the temperature for the energy equation and U the electric potential for the charge equation. In the present model, the fluid is assumed to be no effect on the conduction of electric current.

Then, for the electric potential equation,

$$\mathrm{div}\left(\rho\vec{V}\Phi\right) = 0 \quad (12)$$

For the species transport equations, the dilute approximation is applied in laminar flow.

$$\Gamma_i = \rho D_i \quad (13)$$

where D_i is the diffusion coefficient for species i in the mixture. The electric potential equation is shown as follow.

$$\Gamma_\varphi = \sigma \quad (14)$$

Heat and species concentrations change due to the electrochemical reactions, and the variations are brought into the source terms of the governing equations.

The volumetric heat source term S_q is the sum of the ohmic heat source, the chemical reaction heat and the radiant heat exchange.

$$S_q = Q_{ohm} + Q_{chem} + Q_{rad} \quad (15)$$

where ohmic heat source is:

$$Q_{ohm} = \sigma \mathrm{grad}\Phi \mathrm{grad}\Phi \quad (16)$$

The chemical heat source for the control volume element in the anode side interlayer domain is:

$$Q_{chem,a} = \left(\dot{r}_f - \dot{r}_b\right)\Delta H_s + \dot{r}_R\Delta H_R + \frac{\left|\vec{i}\cdot\vec{n}\right|}{2F}A_{CV}\Delta H_E \quad (17)$$

where in other areas, $Q_{chem} = 0$.

The discrete ordinates radiation model (DTRM) is applied to calculate the radiant heat exchange [22]. The equation for the change of radiant intensity, dI, along a path, ds, can be written as

$$\frac{dI}{ds} + aI = \frac{a\sigma T^4}{\pi} \quad (18)$$

where a stands for the gas absorption coefficient, T the gas local temperature and σ Stefan–Boltzmann constant (5.672×10^{-8} W/m^2 K^4).

The porous media is modeled by the momentum source term to the standard fluid flow equations. The source term consisting of viscous loss term and an inertial loss term can be calculated by the equation:

$$S_j = -\left(\sum_{k=1}^{3} D_{j,k}\mu V_k + \sum_{k=1}^{3}\zeta_{j,k}\frac{1}{2}\rho\left|\vec{V}\right|V_k\right) \quad (19)$$

In the present model, the porous electrodes are simply considered as homogenous and the inertial resistance factor ζ can be considered as zero. The porous electrodes model can be described by Darcy's Law

$$S_j = -\frac{\mu}{\alpha} V_j \tag{20}$$

where α is the permeability of porous material.

The potential is continuous throughout the electric fields except for the electrolyte interfaces where the chemical reactions occur. As shown in Fig. 2, the ionic current density through the electrolyte can be obtained by the following equation

$$\vec{i} \cdot \vec{n} = \frac{E_n - (\Phi_{P'} - \Phi_P)}{R_n} \tag{21}$$

where R_n is the local lumped area specific electric resistance for the sum of polarization.

The thermal flux and electric current flux are zero at the external boundary. Uniform potential is given at the current inlet and outlet as assumed value. The pressure is given at the gas outlets. The temperature, the species mass fractions and the mass fluxes are imposed at the gas inlets.

2.4. Thermal stress model

In the classical theory of linear thermoelasticity (Duhamel–Neumann's law), the components of the strain tensor ε_{ij} are linear functions of the components of the stress tensor and the components of the strain tensor due to the temperature change; that is [23]

$$\varepsilon_{ij} = \varepsilon_{ij}^e + \varepsilon_{ij}^T \tag{22}$$

where ε_{ij}^e denotes the elastic strain and ε_{ij}^T stands for the thermal strain. When temperature changes from T_0 to T, the thermal strain of the element due to the temperature change is

$$\varepsilon_{ij}^T = \alpha(T - T_0)\delta_{ij} \tag{23}$$

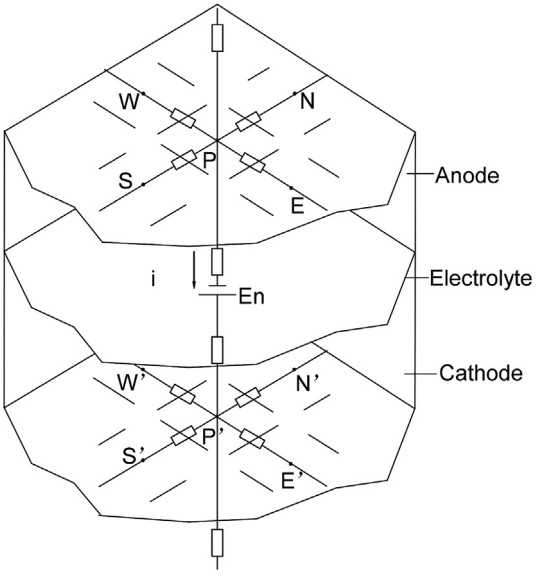

Fig. 2. The grid scheme for computation of current density at electrode/electrolyte interfaces.

Table 1
Basic physical parameters for the SOFC materials [13,14,24,25].

	T/K	E/GPa	ν	$CTE/10^{-6}$ k^{-1}	σ_y/MPa
Cathode (LSM)	RT	41.3	0.28	12.16	–
	1073	48.3	0.28		
Electrolyte (YSZ)	RT	196.3	0.32	10.21	–
	1073	148.6	0.32		
Anode (NiO–YSZ)	RT	124.9	0.39	12.37	–
	1073	119.9	0.39		
Anode (Ni–YSZ)	RT	72.5	0.39	12.41	–
	1073	58.1	0.39		
MIC (Crofer22APU)	RT	216	0.3	11.80	248
	1073	65.9	0.3		35

where α is the coefficient of linear thermal expansion and δ_{ij} is the Kronecker delta. The elastic strain tensor is linearly proportional to the stress tensor as

$$\varepsilon_{ij}^e = \frac{1}{2G}\left(\sigma_{ij} - \frac{\nu}{1+\nu}\sigma_{kk}\delta_{ij}\right) \tag{24}$$

where G is the shear modulus and ν is Poisson's ratio. And the total strain tensor is

$$\varepsilon_{ij} = \frac{1}{2G}\left(\sigma_{ij} - \frac{\nu}{1+\nu}\sigma_{kk}\delta_{ij}\right) + \alpha(T - T_0)\delta_{ij} \tag{25}$$

Eq. (25) is called the constitutive law of linear thermoelasticity. Solving this equation for the stress tensor σ_{ij} gives

$$\sigma_{ij} = 2G\left[\varepsilon_{ij} + \frac{\nu}{1-2\nu}\left(\varepsilon_{kk} - \frac{1+\nu}{\nu}\alpha(T - T_0)\right)\delta_{ij}\right] \tag{26}$$

The stress–strain relations in terms of Young's modulus and Poisson's ratio are frequently used, and they are

$$\begin{aligned}
\varepsilon_{xx} &= \tfrac{1}{E}\left[\sigma_{xx} - \nu(\sigma_{yy} + \sigma_{zz})\right] + \alpha(T - T_0)\\
\varepsilon_{yy} &= \tfrac{1}{E}\left[\sigma_{yy} - \nu(\sigma_{zz} + \sigma_{xx})\right] + \alpha(T - T_0)\\
\varepsilon_{zz} &= \tfrac{1}{E}\left[\sigma_{zz} - \nu(\sigma_{xx} + \sigma_{yy})\right] + \alpha(T - T_0)\\
\varepsilon_{xy} &= \tfrac{\sigma_{xy}}{2G}\\
\varepsilon_{yz} &= \tfrac{\sigma_{yz}}{2G}\\
\varepsilon_{zx} &= \tfrac{\sigma_{zx}}{2G}
\end{aligned} \tag{27}$$

In isotropic material without mechanical loads and temperature distribution, each element expands uniformly in every dimension. In SOFC, the components expansions are different due to the CTE mismatches between the cell components. Under the constraints of the interfaces, thermal stresses are generated to keep the size and interface continuous.

The characteristics of thermal stresses in SOFC PEN structure are calculated from the simulated temperature distribution in SOFC using the SOFC thermal stress finite-element model developed by the commercial finite element software Abaqus. In the stress calculation, the element type C3D8R (3D elements of eight-node linear brick) is employed to create the meshes for the SOFC thermal stress model. The temperature distribution calculated by the SOFC thermal-fluid model is read into the Abaqus as the predefined temperature field. In the stress calculation, it's assumed that no mechanical loads are put on the fuel cell components and the components could deform freely. The available data of mechanical properties for SOFC stack materials is scarce. A linear elastic behavior is assumed for all ceramic components. Plasticity with isotropic hardening and von Mises yield criterion is used for the MIC. The basic physical parameters for the materials of SOFC components used in this model are listed in Table 1 [13,14,24,25].

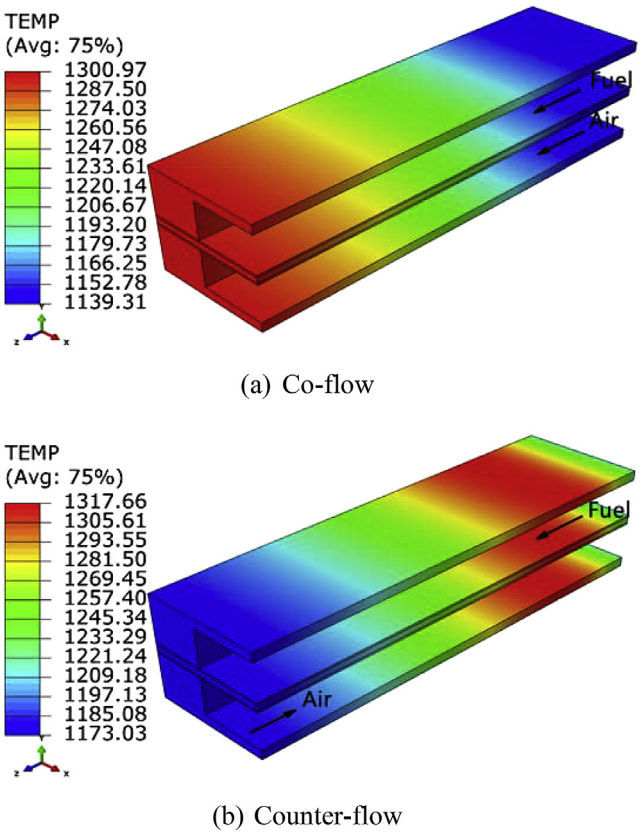

Fig. 3. The calculated profiles of temperature in the cell (a) Co-flow, (b) Counter-flow (T/K).

3. Results and discussion

3.1. Thermo-fluid analysis

Half of the one single symmetric unit cell model with bipolar channels operating with direct internal steam reforming of methane and air in a planar SOFC are modeled in this work. Numerical simulations are performed with both co-flow and counter-flow.

In the former work [17,26], the profile characteristics for the temperature, the electrical potential and the current density calculated by the same model were compared to the benchmark of International Energy Agency (IEA) and showed good agreement with the IEA database [27]. And the comparisons show that the electrochemical model used is accurate in predicting the behavior

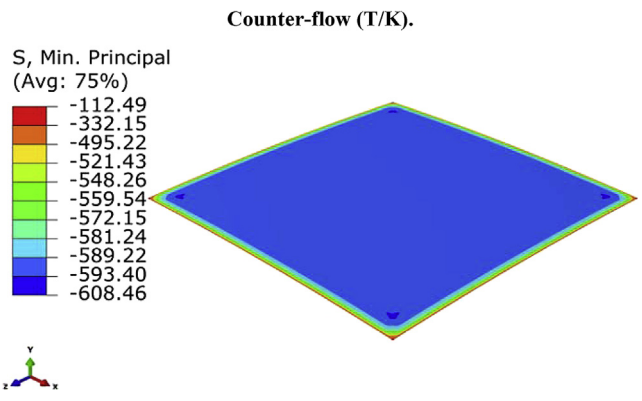

Fig. 4. Simulated stress distribution in the electrolyte at room temperature.

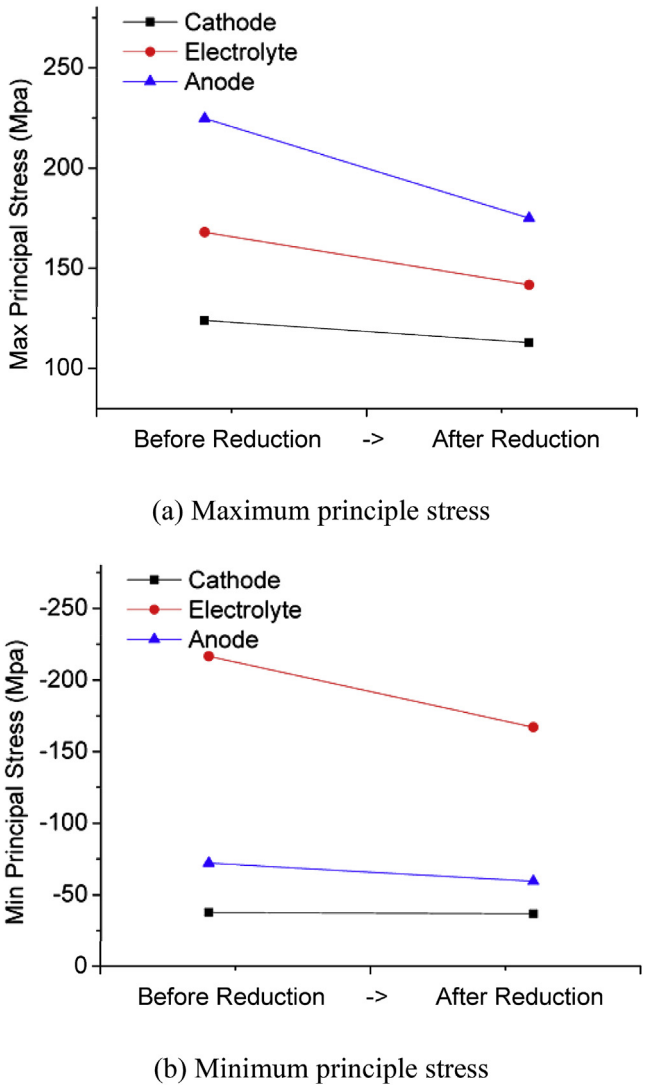

Fig. 5. The residual stresses in the PEN structure before and after the reduction of the anode ($T = 298$ K).

of the SOFC with various geometries. The operating conditions of the case are as follows: system pressure: 1 bar, air ratio: 7, fuel utilization: 85%, the mean current density: 3000 A/m^2, and cell operating voltage: co-flow 0.65 V, counter-flow 0.69 V.

The profile characteristics for temperature are shown in Fig. 3(a) and (b). In the co-flow case, it can be seen that the temperature drops at a short distance from the gas inlet because of the endothermic internal steam reforming reaction of methane. And then the temperature increases toward the gas outlet as the stream reforming reaction is complete. In the counter-flow case, the temperature increases rapidly at fuel inlet because of the exothermic electrochemical reaction and the heated air through the air channel. At the downstream of fuel, the cell temperature decreases along the fuel stream, since the heat generation is small and the hot fuel is cooled by the incoming air.

3.2. Thermal stress calculation

A 3D FEA model consists of positive electrode–electrolyte–negative electrode (PEN) and interconnects assembly is constructed by using commercial finite-element software Abaqus. Thermal stresses in SOFC are calculated in different conditions. The

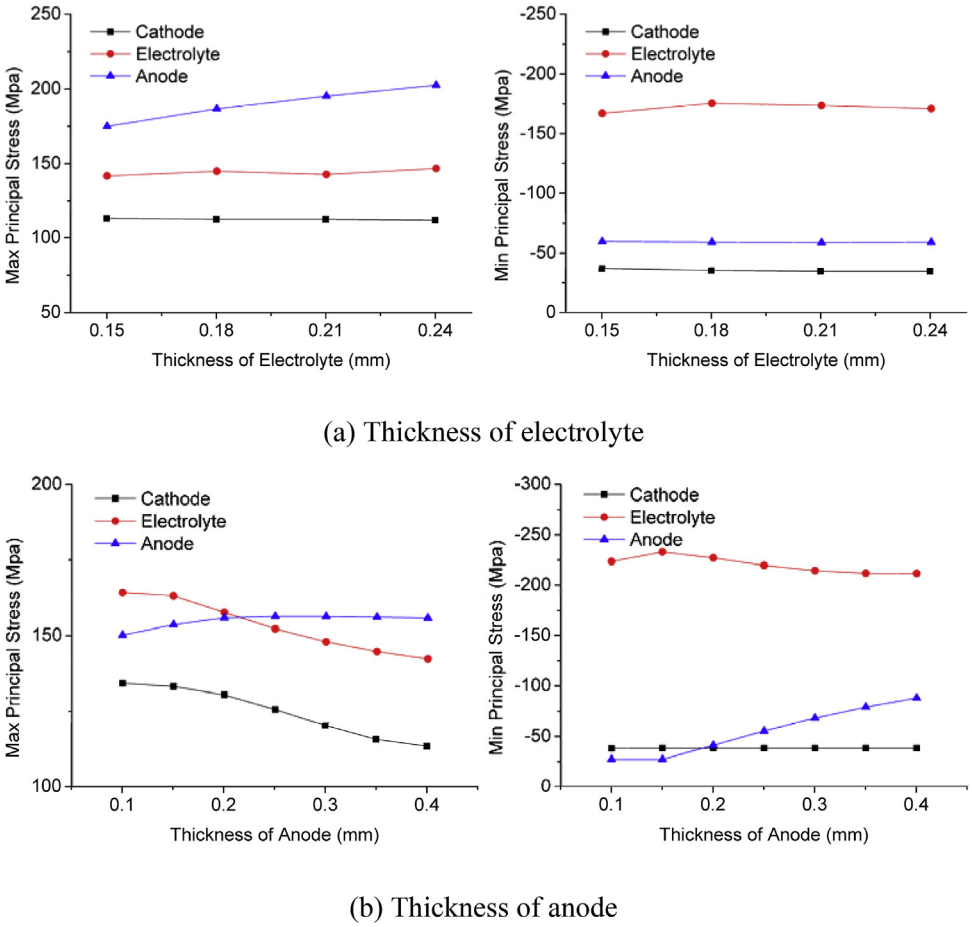

Fig. 6. The relationship between the residual stresses and the thicknesses of different components of PEN ($T = 298$ K).

simulated temperature profile for both co-flow and counter-flow in the planar SOFC are employed in the model. The profile characteristics of stresses in the PEN structure are investigated in particular as the PEN structure materials are normally brittle ceramics. Large thermal stresses will properly lead to the cracks or damage in the PEN structure of SOFC. However, a linear elastic behavior is assumed for the PEN structure and a plastic behavior is used for the MIC, as a consequence it may result in higher cell curvature and different deformation of the SOFC.

In order to justify the accuracy of the FEA model, a SOFC model was constructed in the same way according to the experiment sample in the reference [8]. As shown in Fig. 4, the simulated stress distribution in the electrolyte at room temperature is calculated. The compressive stresses are almost homogeneous values of -560 MPa to -610 MPa over the electrolyte plane except for the edge part. The maximum stress value is −610 MPa which is about 8% smaller than the stress (about −670 MPa) reported in the reference. Near the corner part the stress is slightly larger than that at the center part, which is qualitatively consistent with the result of the X-ray stress measurements in the reference too.

The PEN structure sintering temperature is commonly at 1673 K [8]. The NiO in the porous anode is reduced by humidified hydrogen at the temperature of 1073 K for hours. As shown in Fig. 5(a) and Fig. 5(b), the residual stresses at 298 K in the PEN structure caused by the manufacturing before the reduction and after the reduction for anode are calculated. It can be seen from Fig. 5(a) that the residual tensile stresses in the anode are much higher than the stresses in the cathode and electrolyte. The maximum tensile stress in the anode is 224.67 MPa before the reduction of anode and it drops to 174.94 MPa after the reduction. The anode is subjected to large tensile stress during the first cooling from the sintering temperature (1673 K). The cracks could probably appear in the anode structure when the PEN structure is cooled to the room temperature after sintering. As shown in Fig. 5(b), the residual compressive stresses in the electrolyte are much higher than the stresses in the anode and cathode. The maximum compressive stress in the electrolyte changes from −216.67 MPa to −167.05 MPa after the reduction of anode. The electrolyte is subjected to large compressive stress during the cooling from sintering temperature to balance the large tensile stress in the electrodes. The compressive stresses in the electrolyte are much lower than the strength of YSZ. The chemical reduction of NiO to Ni in the porous of anode lowers the absolute stress level in the PEN structure by 20% and in the mean time the strength of the anode becomes lower too.

The relationship between the residual stresses and the thicknesses of different PEN components at 298 K are calculated to investigate the thickness influences of different PEN components on the residual stresses. As shown in Fig. 6(a), the maximum tensile stress in the anode increases with increasing the thickness of electrolyte, while the maximum compressive stress in the electrolyte increases a little and then stay almost constant. The maximum tensile stress in the electrolyte slightly fluctuates around 145 MPa and stress in the cathode remains almost constant at 112 MPa. The maximum compressive stress in the electrodes is much lower than that in the electrolyte. The maximum tensile stress in PEN structure increases from 174.94 MPa to 202.42 MPa as

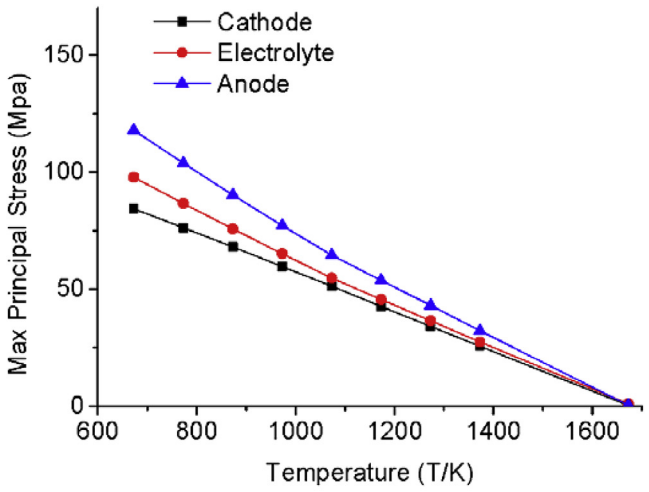

(a) Tensile stresses

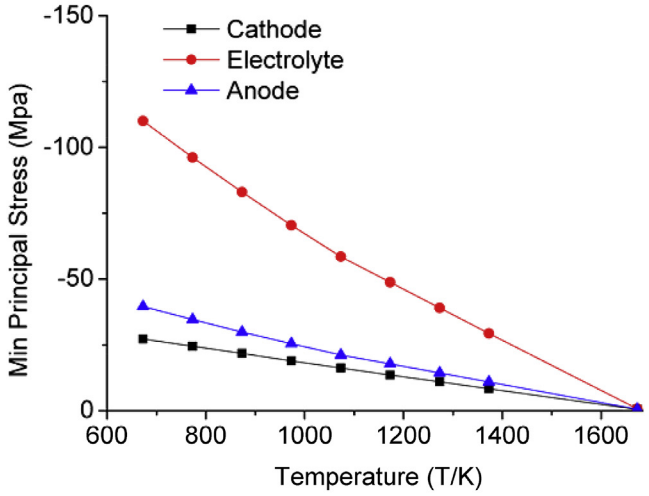

(b) Compressive stresses

Fig. 7. The relationship between the residual stresses and temperature in the PEN structure before the assembly of the MICs.

the thickness of electrolyte increases from 0.15 mm to 0.24 mm. As shown in Fig. 6(b), the residual tensile stresses in the electrolyte and the cathode decrease with the increases of anode thickness. The residual tensile stresses in the anode firstly increase but then decrease a little with increasing the anode thickness. The residual compressive stresses in the electrolyte are much higher than those in the electrodes, which increase a little to −232.96 MPa and then decrease to −211.73 MPa with increasing the anode thickness. The maximum tensile stress in the PEN structure decreases from 164.21 MPa to 155.81 MPa as the thickness of anode increases from 0.1 mm to 0.4 mm. It can be seen from Fig. 6(a) and (b) that both thinner electrolytes and thicker anodes lead to lower residual stresses in the PEN structure. It indicates that thinner electrolytes and thicker anodes are good to the electrolyte-supported SOFC structural performance and reliability.

The distributions of the maximum principal stresses and the minimum principal stresses in PEN structure before the assembly of MICs are calculated at different temperature distributions. As shown in Fig. 7, both the tensile stresses and the compressive stresses decrease almost linearly as the temperature increases from

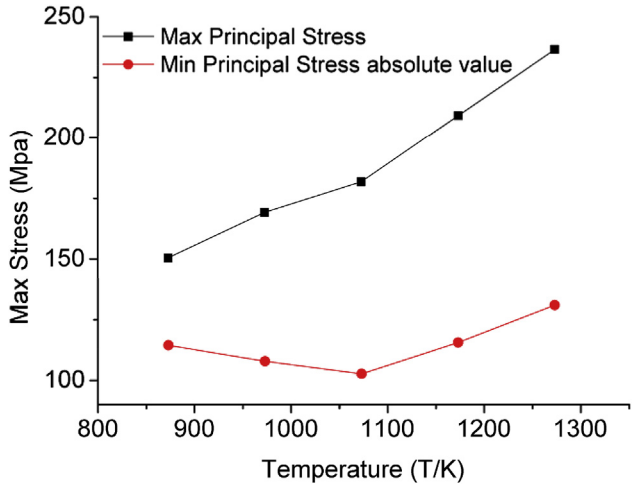

Fig. 8. The relationship between max stresses and temperature.

673 K to 1373 K. The tensile stresses in the anode are larger than those in the electrolyte and cathode while the electrolyte is subjected to the much lager compressive stresses than the other components. Both the tensile stresses and the compressive stresses in the PEN structure are nearly relaxed to zero as the temperature increases to the sintering temperature of PEN structure at 1673 K.

After the assembly of MICs at room temperature, the distributions of the maximum principal stresses and minimum principal stresses in the SOFC are calculated at different temperature distributions. As shown in Fig. 8, the maximum tensile stresses increase with increasing the temperature from 873 K to 1273 K. The maximum compressive stress that the electrolyte is subjected to is −167.05 MPa at room temperature. It decreases to −102.74 MPa as the temperature increases from room temperature to 1073 K. Then it increases to −131.04 MPa with the temperature increasing to 1273 K. Fig. 9 shows the calculated maximum principal stresses at different temperatures for each component. The thermal stresses in the electrolyte are larger than those of other components in uniform temperature distributions. As the temperature increases from 873 K to 1273 K, the maximum principal stresses in the electrolyte increase from 150.43 MPa to 236.53Mpa while the maximum principal stresses in MIC slightly fluctuate around 46 MPa. This is because the coefficients of thermal expansion (CTE)

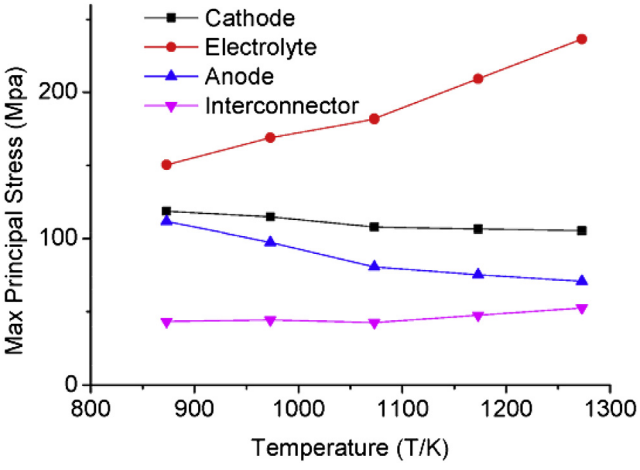

Fig. 9. The relationship between Max Principal stresses and temperature in SOFC structure.

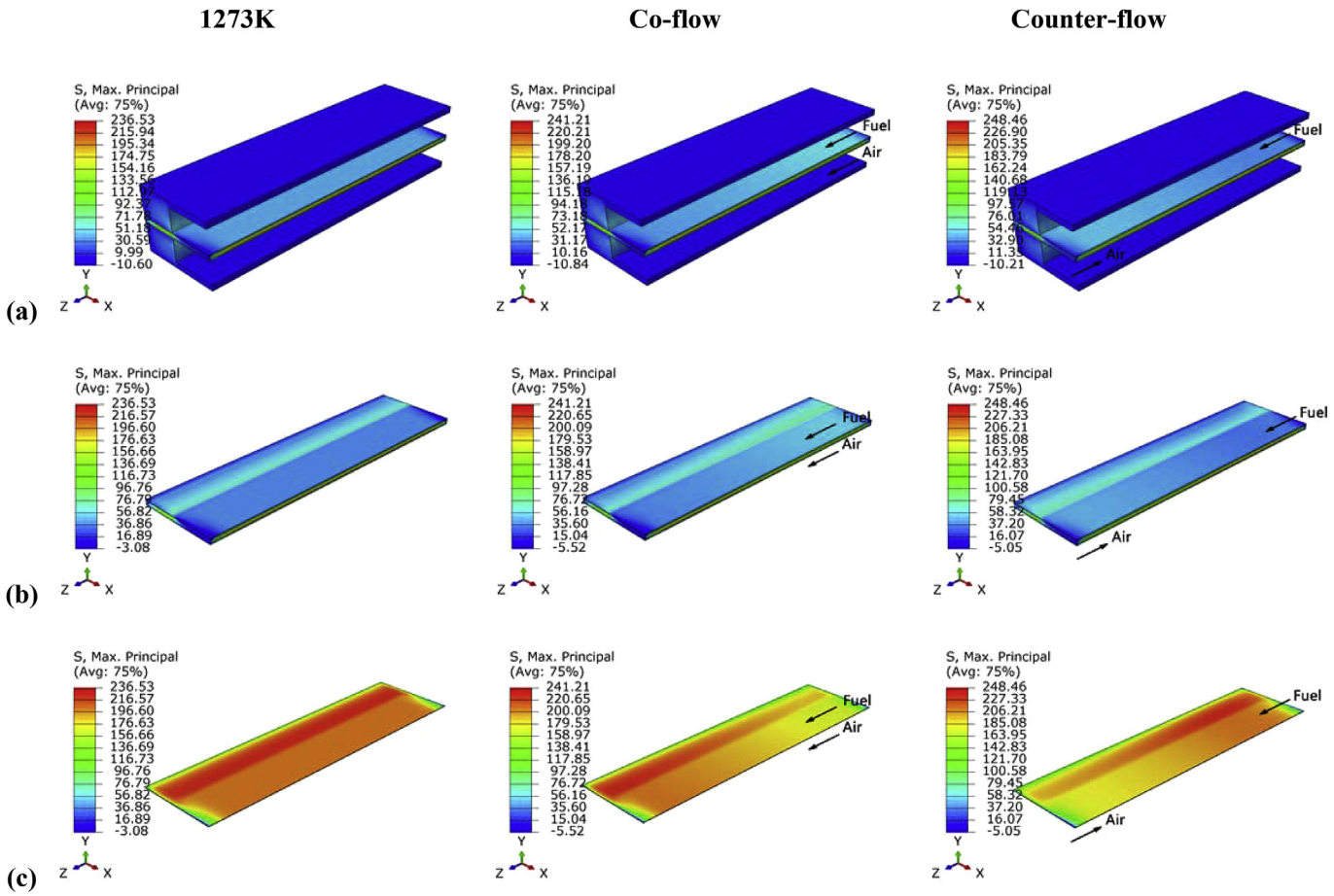

Fig. 10. Max Principal stresses in (a) SOFCs, (b) PEN structures and (c) electrolytes for 1273 K Co-flow and Counter-flow cases.

mismatches between electrolyte and electrodes are comparatively large. As the temperature increases, the mismatch of CTE leads to the increases of the deformation with the components and results in larger stresses. It can also be seen that the maximum principal stresses in the anode decrease from 111.5 MPa to 70 MPa and the stresses in the cathode decrease from 118.52 MPa to 105.21 MPa as the temperature increases from 873 K to 1273 K. The results indicate that the compressive stresses in the electrolyte and the tensile stresses in the anode partly relax whereas the tensile stresses in the electrolyte become larger at a higher temperature in SOFC.

The simulated temperature profile in the planar SOFC can be imported into the thermal stresses finite element model. The profile characteristics of thermal stresses in the PEN structure and MICs are calculated for cases of co-flow, counter-flow and uniform temperature field at 1273 K. The distribution of maximum principal stresses of SOFC, PEN structures and electrolytes are presented in Fig. 10. It can be seen from Fig. 10(a) and (b) that the maximum principal stresses are larger in PEN than that of MICs. The stresses in the electrolyte are much higher than other locations for all cases. The maximum principal stresses in the counter-flow are higher than that of co-flow. The stresses at 1273 K are lower than that of both co-flow and counter-flow. In all the cases above, the maximum value of the tensile stresses is 248.46 MPa appearing in the electrolyte of the counter-flow case. This value is smaller than the failure stress of electrolyte (343 MPa) [7].

In the case of SOFC co-flow, as shown in Fig. 10(c), there is a tensile stress concentration in the electrolyte near to the gas outlet since the temperature increases along the gas flow due to the exothermic electrochemical reaction. The maximum principal stress reaches the maximum value in the electrolyte near the fuel outlet. The reason is that the tensile stress increases with the increases of temperature while the temperature reaches the maximum value at the fuel outlet of SOFC in the case of co-flow. The CTE mismatch between electrolyte and electrodes is comparatively larger.

It is noted from Fig. 10(c) that the tensile stress concentration is near to the fuel inlet in the case of counter-flow. This is because the temperature gradient reaches maximum at the fuel inlet. The mismatch of CTE between electrolyte and electrodes is larger compared to that of the others. Additionally, the stress increases with the increases of temperature. Therefore, the maximum value of maximum principal stresses appears in the electrolyte at the location of maximum temperature.

Fig. 11(a) shows the temperature distributions in the center of electrolyte along the fuel flow direction for both cases of co-flow and counter-flow. In the counter-flow case, the temperature increases rapidly near the fuel inlet. A larger temperature gradient around 10 K mm^{-1} is found within this area. The maximum principal stress distributions along the fuel flow direction are shown in Fig. 11(b). In the co-flow case, the maximum principal stress increases since the temperature increases along the fuel flow direction. The stress reaches maximum near the fuel outlet. In the counter-flow case, the maximum principal stress increases rapidly near the fuel inlet since the high temperature gradient appears in this area. The maximum principal stress reaches maximum at a little ahead of the position where the highest temperature appears. It is indicated that both higher temperature and larger temperature gradient lead to larger tensile stresses. This

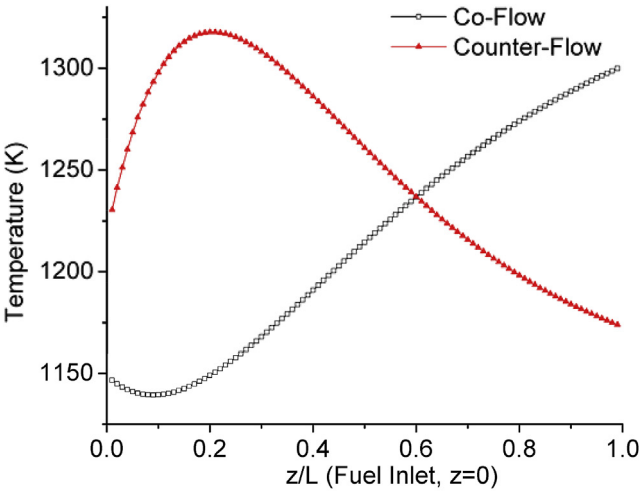

(a) Temperature

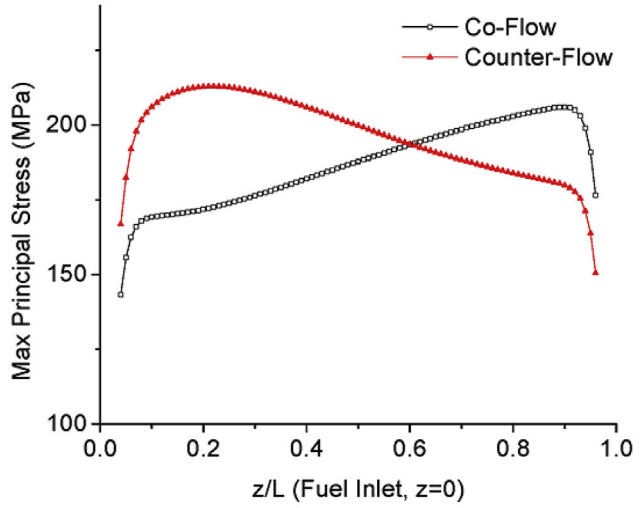

(b) Max Principal thermal stresses

Fig. 11. Max Principal stresses and temperature in the center of the electrolyte along the fuel flow direction.

means the operation temperature and temperature gradient should be reduced in SOFCs to lower the thermal stress.

4. Conclusions

A 3D complete polarization electrochemical model and a thermal stress finite-element model for a planar SOFC are employed in this paper. The internal reforming reaction and water-gas shift reaction are taken into account in the simulations for both co-flow and counter-flow. With the simulated temperature profile in the planar SOFC, the finite-element analysis is employed to calculate the thermal stress distribution in the planar SOFC. The effects of temperature profile, anode and electrolyte thicknesses and coefficients of thermal expansion mismatch between components are characterized and analyzed.

The thermo-fluid simulation results indicated that the temperature gradient near the fuel inlet for counter-flow pattern is much larger than that of co-flow pattern. The thermal stress is mainly contributed by the reason of CTE mismatches between different materials. The anode is subjected to large tensile stress and the electrolyte is subjected to large compressive stresses during the first cooling from the sintering temperature. The cracks could probably appear in the anode structure when the PEN structure is cooled to room temperature after the sintering. The chemical reduction of NiO to Ni in the porous anode lowers the absolute stress level in the PEN structure by 20% while in the mean time the strength of the anode becomes lower too. When the SOFC works at a high temperature, the tensile stresses in the anode and the compressive stresses in the electrolyte relax partly.

Thicker electrolyte leads to larger residual tensile stresses in the anode. The residual compressive stresses in the electrolyte are the maximum among the components of PEN structure. The maximum tensile stress in the PEN structure decreases firstly but then stays stable with increasing the thickness of anode. Both the tensile stresses and the compressive stresses relax as the temperature increases before the assembly of MICs. After the assembly of MICs, the compressive stresses in the electrolyte and the tensile stresses in the anode partly relax whereas the tensile stresses in the electrolyte become larger at a higher temperature in SOFC. The operation temperature and the temperature gradient are the main factors that cause the tensile stress concentration in the electrolyte. As a larger tensile stress may lead to the cracks in the anode, lower operation temperature gradient, close CTE materials and thinner electrolyte are recommended to achieve better performance and higher reliability for SOFCs.

Acknowledgments

This work is supported by the National Natural Science Foundation of China (Grant No. 51276145).

Nomenclature

A_0	the coefficient of conductivity
c_p	specific heat capacity, J mol^{-1} K
D	diffusion coefficient, m^2 s^{-1}
E	activation energy, J mol^{-1}
E_v	voltage, V
E_n	Nernst potential, V
E	Young modulus, Pa
F	Faraday constant, 96485C mol^{-1}
g	molar Gibbs free energy, J mol^{-1}
G	shear modulus, Pa
h	molar enthalpy, J mol^{-1}
i	current density, A m^{-2}
i_0	exchange current density, A m^{-2}
K	equilibrium constant
l	distance, m
L	the length of cell, m
$\vec{n}$	the unit normal vector of reaction interface
p	pressure, Pa
P_0	standard pressure, Pa
P	evaluation value of pressure, Pa
Q	heat source, W m^{-3}
r	area-specific resistance, Ω m^{-2}
$\dot{r}$	volumetric reaction rate, mol s^{-1} m^{-3}
R	universal gas constant, 8.314 J mol^{-1} K^{-1}
R_n	ohmic resistance, Ω
s	molar entropy, J mol^{-1} K^{-1})
S	source component
T	temperature, K
V	velocity, m s^{-1}
z_e	electrons transferred per reaction

Greek letters

α	coefficient of linear thermal expansion, K^{-1}
β	current transfer coefficient
η	polarization, V
ρ	fluid density, kg m^{-3}
σ	conductivity, S m^{-1}
Φ	electric potential, V
ζ	inertial resistance factor
λ	stoichiometric reaction coefficient
γ	coefficient in Eqs. (3) and (4)
μ	fluid viscosity, Pa s
ε_{ij}	strain tensor
σ_{ij}	stress tensor, Pa
σ_y	elastic limit, Pa
ν	Poisson's ratio

Subscript

a	anode
act	activation
b	back
c	cathode
conc	concentration
el	electrolyte
f	forward
i	chemical species
j	direction of coordinate
ohm	ohmic
p	product
r	reactant
rad	radiant
ref	reference

References

[1] U. Pasaogullari, C.Y. Wang, Computational fluid dynamics modeling of solid oxide fuel cells, in: Proc. Electrochem. Soc. (Solid Oxide Fuels Cells VIII, Paris), 7, 2003, p. 1403.

[2] P.W. Li, K. Suzuki, Numerical modeling and performance study of a tubular SOFC, J. Electrochem. Soc. 151 (2004) A548.

[3] R.J. Braun, Optimal Design and Operation of Solid Oxide Fuel Cell Systems for Small-scale Stationary Applications, University of Wisconsin, Madison, 2002.

[4] J.R. Ferguson, J.M. Fiard, R. Herbin, Three-dimensional numerical simulation for various geometries of solid oxide fuel cells, J. Power Sources 58 (1996) 109–122.

[5] H. Yakabe, T. Ogiwara, M. Hishinuma, I. Yasuda, 3-D model calculation for planar SOFC, J. Power Sources 102 (2001) 144–154.

[6] J. Malzbender, R.W. Steinbrech, Advanced measurement techniques to characterize thermo-mechanical aspects of solid oxide fuel cells, J. Power Sources 173 (2007) 60–67.

[7] A. Selcuk, G. Merere, A. Atkinson, The influence of electrodes on the strength of planar zirconia solid oxide fuel cells, J. Mater. Sci. 36 (2001) 1173–1182.

[8] H. Yakabe, Y. Baba, T. Sakurai, Y. Yoshitaka, Evaluation of the residual stress for anode-supported SOFCs, J. Power Sources 135 (2004) 9–16.

[9] W. Fischer, J. Malzbender, G. Blass, R. Steinbrech, Residual stresses in planar solid oxide fuel cells, J. Power Sources 150 (2005) 73–77.

[10] A. Selimovic, M. Kemm, T. Torisson, M. Assadi, Steady state and transient thermal stress analysis in planar solid oxide fuel cells, J. Power Sources 145 (2005) 463–469.

[11] L. Liu, G.-Y. Kim, A. Chandra, Modeling of thermal stresses and lifetime prediction of planar solid oxide fuel cell under thermal cycling conditions, J. Power Sources 195 (2010) 2310–2318.

[12] J. Laurencin, G. Delette, F. Lefebvre-Joud, M. Dupeux, A numerical tool to estimate SOFC mechanical degradation: case of the planar cell configuration, J. Eur. Ceram. Soc. 28 (2008) 1857–1869.

[13] A. Nakajo, F. Mueller, J. Brouwer, D. Favrat, Mechanical reliability and durability of SOFC stacks. Part I: modelling of the effect of operating conditions and design alternatives on the reliability, Int. J. Hydrogen Energy 37 (2012) 9249–9268.

[14] A. Nakajo, F. Mueller, J. Brouwer, D. Favrat, Mechanical reliability and durability of SOFC stacks. Part II: modelling of mechanical failures during ageing and cycling, Int. J. Hydrogen Energy 37 (2012) 9269–9286.

[15] K.S. Weil, B.J. Koeppel, Thermal stress analysis of the planar SOFC bonded compliant seal design, Int. J. Hydrogen Energy 33 (2008) 3976–3990.

[16] T.L. Jiang, M.-H. Chen, Thermal-stress analyses of an operating planar solid oxide fuel cell with the bonded compliant seal design, Int. J. Hydrogen Energy 34 (2009) 8223–8234.

[17] X. Zhang, G. Li, J. Li, Z. Feng, Numerical study on electric characteristics of solid oxide fuel cells, Energy Convers. Manage. 48 (2007) 977–989.

[18] S.H. Chan, K.A. Khor, Z.T. Xia, A complete polarization model of a solid oxide fuel cell and its sensitivity to the change of cell component thickness, J. Power Sources 93 (2001) 130–140.

[19] P. Costamagna, K. Honegger, Modeling at solid oxide heat exchanger integrated stacks and simulation at high fuel utilization, J. Electrochem. Soc. 145 (1998) 3995–4007.

[20] E. Achenbach, E. Riensche, Methane/steam reforming kinetics for solid oxide fuel cells, J. Power Sources 52 (1994) 283–288.

[21] W. Tao, Numerical Heat Transfer, Xi'an Jiaotong University Press, Xi'an, 2001, pp. 311–313.

[22] F. Fluent, 6.3 User's Guide, Fluent Inc, 2006.

[23] R.B. Hetnarski, M.R. Eslami, Thermal Stresses – Advanced Theory and Applications, Springer London, Limited, 2008.

[24] L. Petruzzi, S. Cocchi, F. Fineschi, A global thermo-electrochemical model for SOFC systems design and engineering, J. Power Sources 118 (2003) 96–107.

[25] A. Nakajo, J. Kuebler, A. Faes, U.F. Vogt, H.J. Schindler, L.-K. Chiang, S. Modena, T. Hocker, Compilation of mechanical properties for the structural analysis of solid oxide fuel cell stacks. Constitutive materials of anode-supported cells, Ceram. Int. 38 (2012) 3907–3927.

[26] X. Zhang, J. Li, G. Li, Z. Feng, Numerical study on the thermal characteristics in a tubular solid oxide fuel cell with indirect internal reformer, Int. J. Therm. Sci. 48 (2009) 805–814.

[27] E. Achenbach, SOFC Stack Modeling, in: Final Report of Activity A2, Annex II: Modelling and Evaluation of Advanced Solid Oxide Fuel Cells, in,, Juelich, Germany, March, 1996.